J Mol Model (2009) 15:1245–1252
DOI 10.1007/s00894-009-0452-y

ORIGINAL PAPER

Insights into the functional role of protonation states in the HIV-1 protease-BEA369 complex: molecular dynamics simulations and free energy calculations

Jianzhong Chen · Maoyou Yang · Guodong Hu · Shuhua Shi · Changhong Yi · Qinggang Zhang

Received: 19 October 2008 / Accepted: 16 December 2008 / Published online: 18 March 2009

Abstract The molecular mechanics Poisson-Boltzmann surface area (MM-PBSA) method combined with molecular dynamics (MD) simulations were used to investigate the functional role of protonation in human immunodeficiency virus type 1 (HIV-1) protease complexed with the inhibitor BEA369. Our results demonstrate that protonation of two aspartic acids (Asp25/Asp25′) has a strong influence on the dynamics behavior of the complex, the binding free energy of BEA369, and inhibitor–residue interactions. Relative binding free energies calculated using the MM-PBSA method show that protonation of Asp25 results in the strongest binding of BEA369 to HIV-1 protease. Inhibitor–residue interactions computed by the theory of free energy decomposition also indicate that protonation of Asp25 has the most favorable effect on binding of BEA369. In addition, hydrogen-bond analysis based on the trajectories of the MD simulations shows that protonation of Asp25 strongly influences the water-mediated link of a conserved water molecule, Wat301. We expect that the results of this study will contribute significantly to binding calculations for BEA369, and to the design of high affinity inhibitors.

Keywords Protonation · HIV-1 protease · Molecular dynamics · MM-PBSA method · Binding free energy

J. Chen · M. Yang · G. Hu · S. Shi · C. Yi · Q. Zhang (✉)
College of Physics and Electronics, Shandong Normal University, Jinan 250014, China
e-mail: zhangqg@sdnu.edu.cn

Introduction

The human immunodeficiency virus type 1 (HIV-1) protease (PR), which is responsible for processing viral polyproteins to produce structural and functional proteins, is one of the most important enzymes playing a major role in the life cycle of the HIV virus. PR is a homodimer composed of two identical 99-amino-acid subunits that form a hydrophobic binding pocket with an active site formed by two aspartic acids (Asp25/Asp25′) located at the interface between the two monomers [1]. Flaps positioned over the active site undergo major structural rearrangements upon binding of either a substrate or an inhibitor. The binding of HIV-1 protease inhibitors (PIs) to PR can inhibit the activation of the protease and inhibit replication [2] of HIV. Thus, over the years, PR has become one of the primary targets for developing anti-HIV therapeutics.

The binding triad (Asp25/Asp25′-Thr26/Thr26′-Gly27/Gly27′) located in the active site is stabilized by a network of hydrogen bonds known as the "fireman's grip" [3]. Residues Asp25/Asp25′ are known as the catalytic aspartic acids. It is important to try to assign the proper protonation state of Asp25/Asp25′ in PI–PR complexes. Different protonation states of Asp25/Asp25′ have been found depending on the structure of the PIs and the local environment in which the PI–PR complex is located [4]. Determination of the protonation states of Asp25/Asp25′ in PR is crucial for high affinity inhibitor design. However, the hydrogen positions in the X-ray structural data are missing, and information about protonation cannot be gained directly from X-ray data, making studies of the protonation states of Asp25/Asp25′ indispensable.

So far, several studies concerning protonation of Asp25/Asp25′ have been carried out. Chen and Tropsha [5] used the free energy perturbation method to calculate binding

affinities of the S and R isomer of U85548E in three protonation states. They concluded that U85548E binds to a monoprotonation state of HIV protease. Wittayanarakul and co-workers [6] applied density functional theory (DFT), ONIOM and molecular mechanics Poisson-Boltzmann surface area (MM-PBSA) methods to a computational study of protonation of Asp25/Asp25′ in the saquinavir-PR complex, and obtained computational results of protonation state to those of Asp25. From NMR experiments, Yamazaki et al. [7] determined the diprotonation state of Asp25/Asp25′ in the presence of inhibitor diol groups, whereas Wang and Kollman [8] obtained the unprotonated form of free PR.

In this work, the protonation states of Asp25/Asp25′ in PR complexed with the inhibitor BEA369 were explicitly assigned into four different ionic states. BEA369 is a diol-based inhibitor that can efficiently inhibit activation of PR [9]. Figure 1 shows the structure of BEA369 and the PR–BEA369 complex. To investigate the influence of protonation of Asp25/Asp25′ on the dynamics characteristics, the water-mediated link between the flaps and BEA369, and the binding of BEA369 to PR, molecular dynamics (MD) simulations of PR–BEA369 complexes in which Asp25/Asp25′ were differently protonated in explicit aqueous solution were carried out. By analysing the structural fluctuation and conformational changes caused by the different protonation states of Asp25/ASP25′, calculating the binding free energies, and determining the inhibitor–residue interaction spectrums, we expect that the following three aims can be achieved: (1) to understand the difference in the dynamic characteristics caused by the different protonation states, (2) to illuminate the shift in the water-mediated link between the flaps and BEA369 produced by the different protonation states, and (3) to estimate the effect of protonation on the binding of BEA369 to PR. We expect this study to contribute significantly to the binding calculation of BEA369 to PR, and also to provide important hints for drug design to optimize the interaction of PIs with PR.

Materials and methods

The crystal structure of HIV-1 PR complexed with the inhibitor BEA369 was obtained from the Protein Data Bank (ID, 1EBY) [9] and used as the starting model for MD simulations. The protonation states of Asp25/Asp25′ were assigned to four different ionic states, including unprotonated (both Asp25 and Asp25′ are not protonated), monoprotonation (either Asp25 or Asp25′ is protonated), diprotonation (protonated at both Asp25 and Asp25′). All of these protonations occur in the OD2 atom of Asp25/Asp25′. In this study, the simulated systems were labeled as unpro, mono25, mono25′ and dipro, respectively. All missing hydrogen atoms of the protein were added using the tleap module in the AMBER 9.0 software package [10]. All the crystal water molecules in the crystal structure of the PR–BEA369 complex were kept in the starting model. The force field ff03 was used to produce the force field parameters for the protein and the crystal water molecules.

The initial coordinates of the inhibitor BEA369 were extracted from 1EBY. The electronic potential of BEA369 was calculated using the Gaussian 98 package at the HF/6-31G** level. The atom-centered partial charges for BEA369 were derived by using the RESP fitting technique [11] in AMBER. Other force field parameters, including the Lennard-Jones, torsion and bond angle terms, were assigned using the antechamber module in AMBER 9.0. In the next step, each PR–BEA369 complex was soaked in a truncated octahedral periodic box of TIP3P water molecules. The minimum distance from the edges of the water box to the closest atom of the complex was 10 Å. An appropriate number of Cl^- ions was added to neutralize the entire system.

Energy minimization and MD simulation were performed using the sander module of AMBER 9.0 to relax the structures and investigate the dynamics of the four complexes. The whole system was subject to energy minimization in two stages to remove bad contacts. Firstly, the solvent

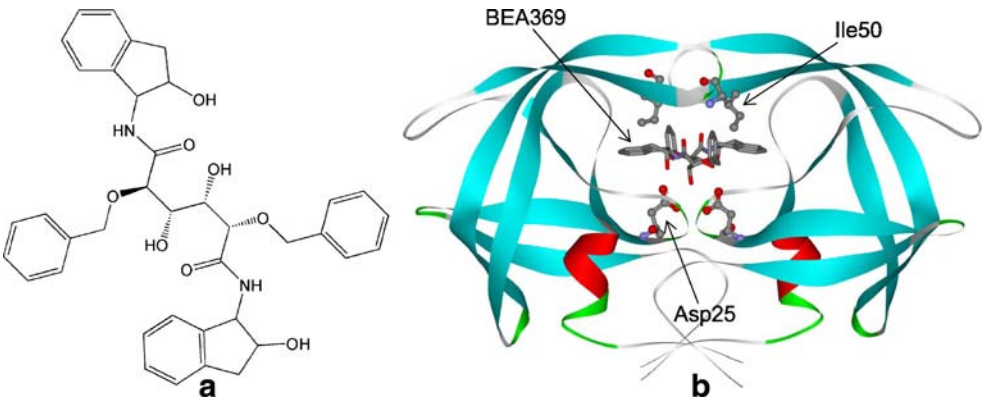

Fig. 1 **a** Molecular diagram of the human immunodeficiency virus type 1 (HIV-1) protease (PR) inhibitor BEA369. **b** Structure of the PR–BEA369 complex. Residues Asp25/Asp25′ at the active site and Ile50/Ile50′ in the flaps are displayed using *ball-and-stick* representation, BEA369 is shown in *stick* representations. Only one subunit is labeled

was minimized by holding the solute fixed using a harmonic constraint with a strength of 100 kcal · mol^{-1} · $Å^{-2}$. Secondly, the entire system was minimized without restriction. Each stage was performed using the steepest descent minimization of 500 steps followed by a conjugate gradient minimization of 2,500 steps.

The MD simulation was carried out by utilizing the periodic boundary condition. Langevin dynamics with a collision frequency of 1.0 ps^{-1} were employed to control the temperature of the system. The SHAKE algorithm [12] was applied to constrain all bonds involving hydrogen. The particle mesh Ewald method [13] was adopted to treat long-range electrostatic interactions. The time step of all MD simulations was 2 fs, with a direct-space, nonbonded cutoff of 10 Å. Initial velocities were assigned from a Maxwellian distribution at the initial temperature.

The MD simulation consists of heating, equilibration and production phases. The system was gradually heated from 0 to 300 K in the first 100 ps. Then, the system was equilibrated at 300 K for another 100 ps. During heating and equilibration, all solute atoms were restricted by a harmonic constraint with a strength of 10 kcal · mol^{-1} · $Å^{-2}$. Finally, 2-ns production phase was performed without restriction at a constant temperature of 300 K and a constant pressure of 1 atm for each system. The MD trajectory was saved every 0.2 ps. Analysis of the root-mean-squared deviation (RMSD) was carried out using the ptraj module of AMBER 9.0 to explore the stability of the system.

The binding free energy of the inhibitor to the protein was calculated using the MM-PBSA method [14–21]. In this approach, frames of a MD trajectory are stripped of Cl^- ions and water molecules, and their binding free energies (ΔG) are approximated by

$$\Delta G = \Delta G_{MM} + \Delta G_{sol} - T\Delta S \quad (1)$$

where ΔG_{MM} is the molecular mechanics free energy in gas phase, ΔG_{sol} is the solvation free energy and $T\Delta S$ is a term involving the entropy effect. The molecular mechanics free energy (ΔG_{MM}) can further be expressed as

$$\Delta G_{MM} = \Delta G_{vdw} + \Delta G_{ele} \quad (2)$$

where ΔG_{vdw} and ΔG_{ele} represent the van der Waals and electrostatic interactions in gas phase, respectively. The solvation free energy (ΔG_{sol}) is further divided into two components:

$$\Delta G_{sol} = \Delta G_{pol} + \Delta G_{nonpol} \quad (3)$$

where ΔG_{pol} and ΔG_{nonpol} are the polar and non-polar contributions to the solvation free energy, respectively. The former component was computed using the pbsa program. The dielectric constant inside the solute was set to 1.0 and 80.0 in the solvent in our calculations. The latter term was determined by

$$\Delta G_{nonpol} = \gamma SASA + \beta \quad (4)$$

where SASA (solvent-accessible surface area) was calculated with the MSMS program [22]. In this work, the values of γ and β was set to 0.00542 kcal mol $Å^{-2}$) and 0.92 kcal mol^{-1}, respectively.

The contributions of entropy ($T\Delta S$) to binding free energy arise from changes in the translational, rotational and vibrational degrees of freedom. $T\Delta S$ are generally calculated using classical statistical thermodynamics [23] and normal-mode analysis. In this work, the entropy effect was not included because the difference in the entropy effect caused by all similar systems is very small.

In order to understand the effect of protonation of Asp25/Asp25′ on the inhibitor–residue interaction, the interaction energy was further decomposed into the contributions from each residue in PR by using the theory of free energy decomposition [24]. These energy decompositions are helpful in understanding whether protonation of Asp25 or Asp25′ is appropriate for the current PR–BEA369 complex.

The hydrogen bonds were analyzed using the ptraj module of AMBER. The formation of hydrogen bonds depends on the criteria of distance and orientation as follows: (1) a distance between proton donor (D) and acceptor (A) atoms shorter than or equal to 3.5 Å, (2) the angle D-H···A is greater than or equal to 120°.

Results and discussion

MD simulations were performed successfully for four systems. To explore the reliable stability of the MD trajectories and to understand the effect of protonation of Asp25/Asp25′ on the stability of MD simulations, the

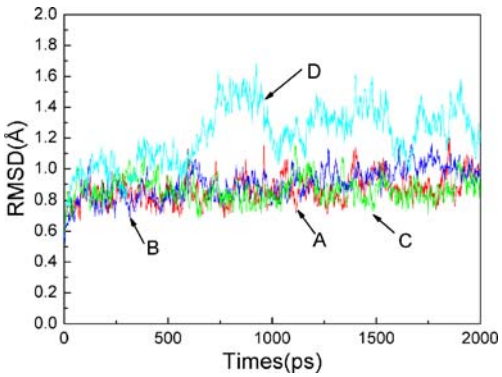

Fig. 2a–d Root-mean-square deviations (RMSD) of C_α atoms of all complexes relative to the initial minimized structure through the production phase. **a** Mono25 (Asp25 protonated), **b** mono25′ (Asp25′ protonated), **c** dipro (protonated at both Asp25 and Asp25′) and **d** unpro (both Asp25 and Asp25′ not protonated)

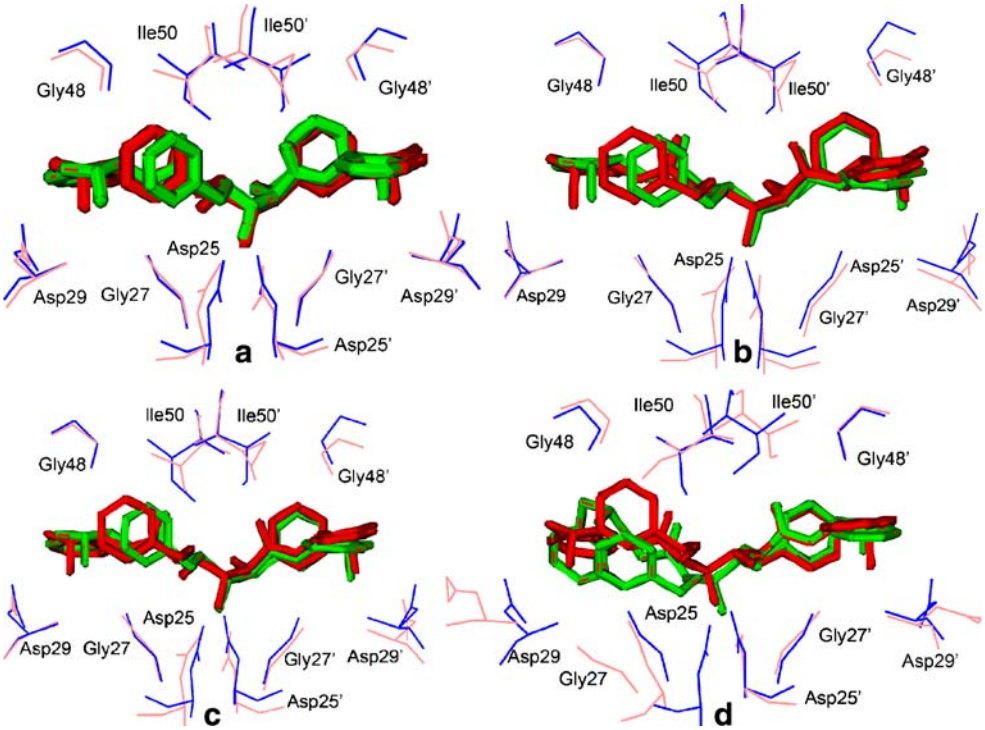

Fig. 3a–d Average structures from the final 400 ps of the molecular dynamics (MD) trajectories of the complex superimposed on the crystal structures via protease backbone atoms. For crystal structures, the protease is shown in *blue* and BEA369 in *red*; for MD structures, the protease is shown in *pink* and BEA369 in *green*. **a** mono25, **b** mono25′, **c** dipro, **d** unpro

RMSD of C_α atoms relative to the initial minimized structure through the production phase were calculated (plotted in Fig. 2). One can see that, in the first 400 ps, the RMSD values increase quickly, meaning that the structures of PR in solution relax and release repulsions within the complexes. From Fig. 2, the mono25, mono25′ and dipro systems had reached equilibrium after 600 ps of the production phase, while the unpro system was not stable until about 1 ns. The RMSD of the unpro system differs from that of the mono25, mono25′ and dipro systems. Moreover, Fig. 2 also indicates that the mono25, mono25′ and dipro systems have similar dynamic behavior; their averaged RMSD values are 0.89, 0.94 and 0.86 Å, respectively, and their deviations from the mean are lower than 0.55 Å, which shows that the trajectories of these systems are stable. However, for the unpro system, the average RMSD value is 1.32 Å and the deviation from the mean is 0.61 Å, which suggests that the stability of the unpro system is poorer than that of mono25, mono25′ or dipro.

Figure 3 shows the superimposition of the crystal structure with the average structures of unpro, mono25, mono25′ and dipro systems during the final 400 ps of the MD trajectories via backbone atoms. One can see that the average structures of the mono25, mono25′ and dipro systems generally agree with the crystal structure; however, the phenyl ring in P1 of the BEA369 shifts slightly. For unpro system shown in Fig. 3(d), P1′ and P2′ of BEA369 as well as chain B of PR also generally agree with the crystal structure, while P1 and P2 of BEA369 and chain A of PR differ from the crystal structure. Perhaps due to the strong electrostatic repulsion between Asp25 and Asp25′, some residues in the unpro system obviously deviate from the crystal structure in the simulation, especially residues Asp25, Gly27 and Asp29 in chain A. In turn, the deviation of these residues also leads to the rearrangement of P1 and P2 in BEA369. This implies that protonation of Asp25 in chain A may remove local structural changes in the PR–BEA369 complex.

To investigate the effect of protonation of Asp25/Asp25′ on the flexibility of PR, the B-factors of the C_α atoms from the backbone of PR during the final 400 ps of the MD trajectories were calculated (plotted in Fig. 4). The B-factor, known as the crystal temperature factor, is generally applied to measure the mobility and flexibility of the structure [25].

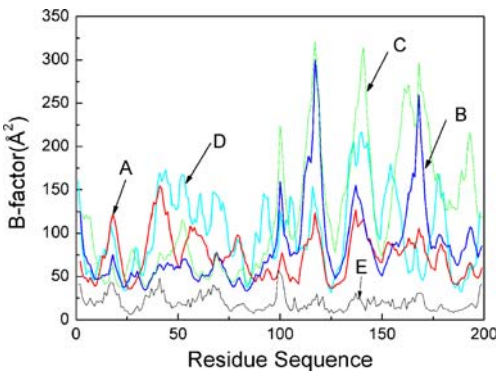

Fig. 4 B-factors of the C_α atoms for each residue of four PR–BEA369 complexes with different protonation states during the final 400 ps of the 2 ns production phase. *Red* (*A*) Mono25, *blue* (*B*) dipro, *green* (*C*) mono25′, *cyan* (*D*) unpro, *black* (*E*) experimental

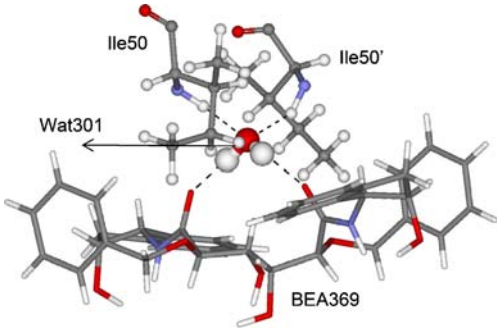

Fig. 5 Hydrogen bonds formed by the crystal water molecule (Wat301) with residues (Ile50/Ile50′) and with BEA369. The residues Ile50/Ile50′ in the flaps and the crystal water molecule Wat301 are displayed using *ball-and-stick* representation, BEA369 is shown in *stick* representation

Figure 4 shows that regions of flexibility in the PR-BEA369 complex occur around residues 17–19, 38–42 55–73 and 92–99 in chain A as well as the corresponding residues in chain B. This result is in accord with previous studies on the flexibility of PR [26, 27]. The calculated values of the B-factors of chain B in the mono25′ and dipro system are much larger than the experimental values. This is probably caused by incorrect protonation of Asp25′, because both the mono25′ and dipro systems relate to protonation of Asp25′. Although the B-factors of chain B in the unpro system are lower than those in the mono25′ and dipro systems, the fluctuation trend of the unpro B-factors disagrees with experimental results. From Fig. 4, one can see that the fluctuation trend of the B-factors in the mono25 system generally agrees with experimental values.

It is well known that the crystal water molecule Wat301 is conserved in all structures of PR complexed with PIs or the substrate, except for structures with PIs such as DMP323 [28, 29] and DMP450 [30] etc. This water molecule (Wat301) can set up a water-mediated link by forming four hydrogen bonds with residues Ile50/Ile50′ and the PIs. Figure 5 displays these four hydrogen bonds in the PR–BEA369 complex. In order to investigate the influence of protonation of Asp25/Asp25′ on these hydrogen bonds, an analysis of hydrogen bonds was performed on the basis of the trajectories of the MD simulations. Table 1 lists the features of these hydrogen bonds.

According to Table 1, during the MD simulations of the four systems, the distance between the N of Ile50/Ile50′ and the O of Wat301 varies in the range of 2.915 Å to 3.095 Å, as the N of Ile50/Ile50′ donates two protons to the O of Wat301 to form two hydrogen bonds, with occupancy rates higher than 70%, which suggests these two hydrogen bonds are stable. Compared with the mono25 system, the occupancy rate of the hydrogen bonds of NH (Ile50′)···O (Wat301) decrease by 14.00%, 17.90% and 7.10% for the mono25′, dipro and unpro systems, respectively, and the occupancy rate of the hydrogen bond of NH (Ile50)···O (Wat301) also decreases by 25.90% for the unpro system, which indicates that the water-mediated link of Wat301 in the mono25′, dipro and unpro systems may become weak. At the same time, two hydrogen bonds between the hydrogen of Wat301 and the carbonyl oxygen of BEA369 are also formed (Table 1). For the mono25 system, the occupancy rate of the hydrogen bonds of OH1 (Wat301) ···O6 (BEA369) and OH2 (Wat301)···O2 (BEA369) are

Table 1 Hydrogen bonds formed by Wat301 with residues Ile50/Ile50′ of human immunodeficiency virus type 1 (HIV-1) protease (PR) and with the inhibitor BEA369. *Mono25* Asp25 protonated, *mono25′* Asp25′ protonated, *dipro* protonated at both Asp25 and Asp25′, *unpro* both Asp25 and Asp25′ not protonated

Protonation	Donor	Acceptor	Distance (Å)	Angle (°)	Occupied (%)
mono25	Wat301-O-H1	BEA369-O6	2.782(0.14)	163.10(9.51)	100
	Wat301-O-H2	BEA369-O2	2.794(0.14)	159.11(11.5)	99.80
	Ile50-N-H	Wat301-O	3.039(0.17)	155.49(12.1)	96.50
	Ile50′-N-H	Wat301-O	3.034(0.16)	153.81(13.6)	92.60
mono25′	Wat301-O-H1	BEA369-O6	2.864(0.17)	159.97(10.7)	24.40
	Wat301-O-H2	BEA369-O2	2.840(0.16)	163.08(9.97)	24.70
	Ile50-N-H	Wat301-O	2.915(0.12)	162.32(9.69)	99.90
	Ile50′-N-H	Wat301-O	3.088(0.17)	152.37(11.4)	78.60
dipro	Wat301-O-H1	BEA369-O6	2.853(0.17)	162.05(10.2)	98.50
	Wat301-O-H2	BEA369-O2	2.874(0.17)	158.44(11.8)	98.30
	Ile50-N-H	Wat301-O	2.944(0.14)	160.47(10.0)	98.40
	Ile50′-N-H	Wat301-O	3.071(0.17)	152.32(14.5)	74.70
unpro	Wat301-O-H1	BEA369-O6	2.812(0.16)	162.38(9.88)	44.90
	Wat301-O-H2	BEA369-O2	2.956(0.23)	158.69(13.2)	38.30
	Ile50′-N-H	Wat301-O	3.038(0.16)	157.59(12.6)	85.50
	Ile50-N-H	Wat301-O	3.095(0.18)	150.50(14.5)	70.60

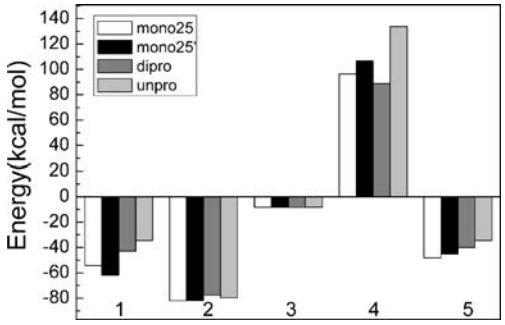

Fig. 6 Binding free energy components (kcal mol^{-1}) of BEA369 to HIV-1 protease calculated by the MM/PBSA method. Components are as follow: *1* electrostatic, *2* van der Waals, *3* nonpolar solvation, *4* polar solvation, *5* total binding free energy

100% and 99.80%, respectively, and the donor–acceptor distances of these two hydrogen bonds are 2.782 Å and 2.794 Å, respectively. In the dipro system, these two hydrogen bonds were found to be similar to those in the mono25 system. Compared with the mono25 system, the occupancy rate of the hydrogen bonds of OH1 (Wat301) ⋯O6 (BEA369) and OH2 (Wat301)⋯O2 (BEA369) in the mono25′ and unpro systems are markedly reduced, reflecting the fact that the strength of these two hydrogen bonds in the mono25′ and unpro systems also weakens. Thus, protonation of Asp25/Asp25′ has a strong influence on the water-mediated link of Wat301, which is in general agreement with the results of Yipin Lu et al. [31]. On the basis of the above analysis, it is concluded that protonation of Asp25 in PR can better maintain the water-mediated link of Wat301 than the other three protonations.

MM-PBSA using the single trajectory method was performed to calculate the binding free energies from the single trajectory of the four systems. A total of 101 snapshots were taken at a time interval of 4 ps from the final 400 ps of MD trajectories for analysis of binding free energies. The calculated binding free energies averaged from these 101 snapshots are shown by Fig. 6. Because differences in the entropy effect can be omitted since the four systems are so similar, the contribution of entropy to binding free energy was not explicitly taken into account in this work.

Figure 6 shows the binding free energies and energy components, i.e., van der Waals, electrostatic, polar solvation and nonpolar solvation components. The van der Waals and electrostatic terms contribute major favorable interactions, whereas polar solvation terms oppose binding. Nonpolar solvation terms, which correspond to the burial of SASA upon binding, contribute in a slightly favorable way. Protonation of Asp25/Asp25′ results in different effects on the separate energy components. As can be seen in Fig. 6, protonation of Asp25/Asp25′ influences slightly van der

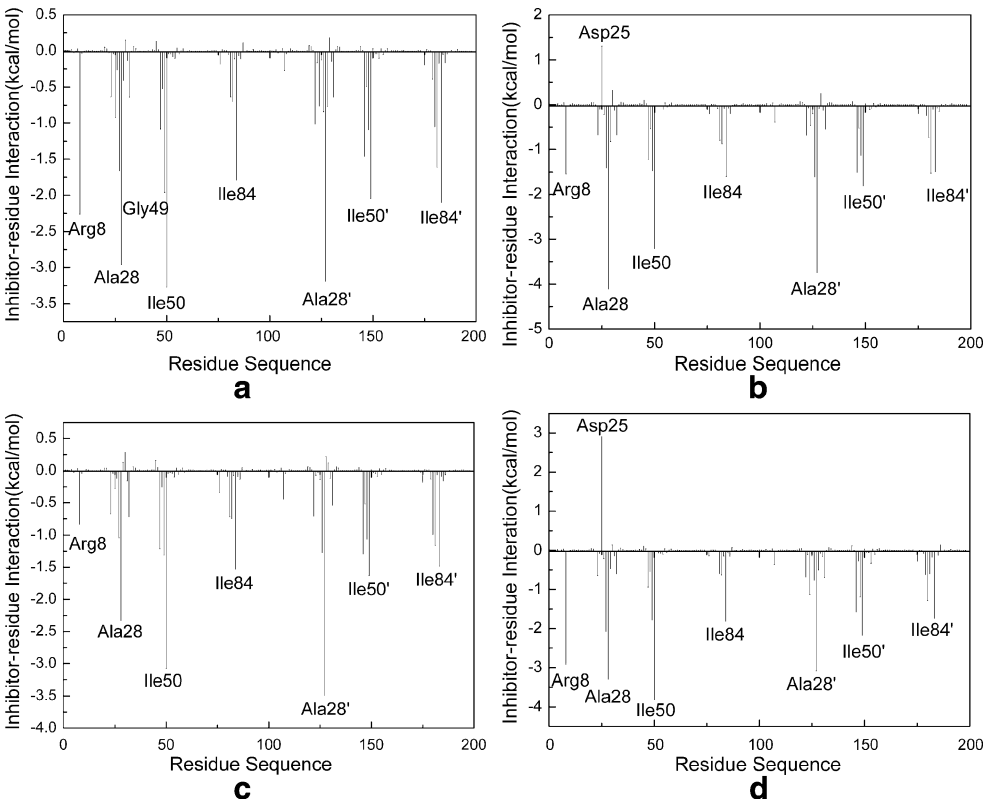

Fig. 7a–d Inhibitor–residue interaction spectrum of PR-BEA369 complexes. *x-Axis* Residue number of PR, *y-axis* interaction energy between BEA369 and specific residues. **a** Mono25, **b** mono25′, **c** dipro, **d** unpro

Waals and nonpolar solvation terms. However, it produces an obvious effect on the electrostatic and polar solvation terms, in particular for the unpro system, and causes a strong polar solvation energy of 133.78 kcal mol^{-1}. One can also see that protonation of Asp25 can produce the strongest binding free energy (−48.20 kcal mol^{-1}) of BEA369 to PR, while unprotonated Asp25/Asp25′ leads to the weakest binding (−34.45 kcal mol^{-1}). It was concluded that protonation of Asp25 was the most favorable protonation state energetically, which is in accord with the calculations of Wittayanarakul and co-workers [6].

Based on analysis of the hydrogen bonds formed by Wat301 and the calculations of binding free energy, it is apparent that protonation of Asp25/Asp25′ has a strong influence on hydrogen bonding, electrostatic interactions and polar solvation free energy, which generally agrees with the pK_a calculations of Davies et al. [32].

In order to gain insight into the effect of protonation of Asp25/Asp25′ on binding at the atomic level, the binding free energy was decomposed into contributions from each residue of PR. The inhibitor–residue interaction spectrums of the four systems are plotted in Fig. 7. It was observed that the different protonations result in distinct influences on the inhibitor–residue interactions. The contributions from individual residues to binding free energies vary with the different protonation states. Residues Arg8, Ala28/Ala28′, Ile50/Ile50′ and Ile84/Ile84′ make a significant contribution in all four systems.

Special attention was paid to residues crucial to inhibitor binding, i.e., the two catalytic aspartic acids Asp25/Asp25′. The total contribution of Asp25/Asp25′ was the most favorable (−1.68 kcal mol^{-1}) in the case of mono25, slightly favorable (−0.31 kcal mol^{-1}) in the case of dipro, moderately repulsive (0.84 kcal mol^{-1}) in the case of mono25′, and the most repulsive (1.76 kcal mol^{-1}) in the case of unpro. According to Fig. 7, Asp25 produces a strong repulsion (2.9 kcal mol^{-1}) for the unpro system, which greatly impairs the binding of BEA369 to PR, also implying that Asp25 may need to be protonated. Protonation of Asp25′ (mono25′ system) also results in a repulsive interaction (1.3 kcal mol^{-1}), and does not completely counteract the repulsion caused by unprotonation, which suggests that protonation of Asp25′ is inapplicable in the context of the current PR-BEA369 complex. Compared to mono25′, protonation of Asp25 and diprotonation of Asp25/Asp25′ have removed entirely the repulsion generated by unprotonation; moreover, the total contribution of Asp25/Asp25′ to binding was favorable. From Fig. 7, one can see that protonation of Asp25 in PR (mono25 system) produces the most favorable effect on the binding of BEA369 to PR, and may be the most applicable to the current complex of the four protonation states examined here.

Conclusions

MM-PB/SA calculations combined with MD simulations were performed to investigate the functional role of protonation of HIV-1 PR in the PR–BEA369 complex. Our results show that protonation of Asp25/Asp25′ has a strong influence on the dynamics behavior of the complex, the binding free energy of BEA369, and inhibitor–residue interactions. Analyses of hydrogen bonds on the basis of the trajectories of MD simulations suggests that protonation also has a strong influence on the role of the water molecule Wat301. Protonation leads to changes in the ionic states of Asp/Asp25′; these changes of ionic states in turn also influence hydrogen bonding, electrostatic interactions and polar solvation energy, as testified by our calculations. To sum up, of the four protonation states examined here, protonation of Asp25 may be the most applicable to the PR–BEA369 complex. We expect this study to contribute significantly towards determining the binding calculation of BEA369, which in turn will inform high affinity inhibitor design.

Acknowledgments This work is supported by the National Nature Science Foundation of China (Grant Nos. 10874104, 10474060 and 10504017), the key Project of Chinese Ministry of Education (NO.206093) and the key Project of Nature Science Foundation of Shandong Province (Z2007A05).

References

1. Nam KY, Chang BH, Han CK, Ahn SK, No KT (2003) Bull Korean Chem Soc 6:817–823
2. Kohl NE, Emini EA, Schleif WA, Davis LI, Heimbach JC, Dixon RA, Scolnick EM, Sigal IS (1988) Proc Natl Acad Sci USA 85:4686–4690
3. Wlodawer A, Vondrasek J (1998) Annu Rev Biomol Struct 27:249–284
4. Smith R, Brereton IM, Chai RY, Kent SBH (1996) Nat Struct Biol 3:946–950
5. Chen X, Tropsha A (1995) J Med Chem 38:42–48
6. Wittayanarakul K, Aruksakunwong O, Saen-oon S, Chantratita W, Parasuk V, Sompornpisut P, Hannongbua S (2005) Biophys J 88:867–879
7. Yamazaki T, Nicholson LK, Torchia DA, Wingfield P, Stahl SJ, Kaufman JD, Eyermann CJ, Hodge CN, Lam PYS, Ru Y (1994) Am Chem Soc 116:10791–10792
8. Wang W, Kollman PA (2000) J Mol Biol 303:567–582
9. Andersson HO, Fridborg K, Lowgren S, Alterman M, Muhlman A, Bjorsne M, Garg N, Kvarnstrom I, Schaal W, Classon B, Karlen A, Danielsson UH, Ahlsen G, Nillroth U, Vrang L, Oberg B, Hallberg B, Samuelsson A, Unge T (2003) Eur J Biochem 270:1746–1758
10. Case DA, Darden TA, Cheatham III TE, Simmerling CL, Wang J, Duke RE, Luo R, Merz KM, Pearlman DA, Crowley M, Walker RC, Zhang W, Wang B, Hayik S, Roitberg A, Seabra G, Wong KF, Paesani F, Wu X, Brozell S, Tsui V, Gohlke H, Yang L, Tan C, Mongan J, Hornak V, Cui G, Beroza P, Mathews DH, Schafmeister C, Ross WS, Kollman PA (2006) AMBER 9 University California, San Francisco

11. Cieplak P, Cornell WD, Bayly C, Kollman PA (1995) J Comput Chem 16:1357–1377
12. Ryckaert JP, Ciccotti G, Berendsen JC (1977) J Chem Phys 23:327–341
13. Darden T, York D, Pedersen L (1993) J Chem Phys 98:10089–10092
14. Li T, Matheus M, Herdewijn P (2008) J Mol Graphics Model 26:813–823
15. Hou T, Yu R (2007) J Med Chem 50:1177–1188
16. Xu Y, Wang R (2006) Proteins 64:1058–1068
17. Kuhn B, Gerber P, Schulz-Gasch T, Stahl M (2005) J Med Chem 48:4040–4048
18. Zhuang S, Zou J, Jiang Y, Mao X, Zhang B, Liu L, Yu Q (2005) J Med Chem 48:7208–7214
19. Wang J, Morin P, Wang W, Kollman PA (2001) J Am Chem Soc 123:5221–5230
20. Fogolari F, Brigo A, Molinari H (2003) Biophys J 85:159–166
21. Reyes CM, Kollman PA (2000) J Mol Biol 297:1145–1158
22. Sanner MF, Olson AJ, Spehner J (1996) Biopolymers 38:305–320
23. McQuarrie DA (1976) Statistical mechanics. Harper and Row, New York
24. Gohlke H, Kiel C, Case DA (2003) J Mol Biol 330:891–913
25. Yang R, Lee MC, Yan H, Duan Y (2005) Biophys J 89:95–106
26. Piana S, Carloni P, Rothlisberger U (2002) Protein Sci 11:2393–2402
27. Zoete V, Michielin O, Karplus M (2002) J Mol Biol 315:21–52
28. Lam PYS, Jahdav PK, Eyermann CJ, Hodge CN, Ru Y, Meek LT, Bacheler JL, Otto MJ, Rayner MM, Wong YN, Chang CH, Weber PC, Jackson DA, Sharpe TR, Erickson-Viitanen S (1994) Science 263:380–384
29. Lam PYS, Ru Y, Jahdav PK, Aldrich PE, DeLucca GV, Eyermann CJ, Chang CH, Emmett G, Holler ER, Daneker WF, Li L, Confalone PN, McHugh RJ, Han Q, Li R, Markwalder JA, Seitz SP, Sharpe TR, Bacheler LT, Rayner MM, Klabe RM, Shum L, Winslow DL, Korhauser DM, Jackson DA, Erickson-Viitanen S, Hodge CN (1996) J Med Chem 39:3514–3525
30. Hodge CN, Aldrich PE, Bacheler LT, Chang CH, Eyermann CJ, Garber S, Grubb M, Jackson DA, Jadhav PK, Korant B, Lam PY, Maurin MB, Meek JL, Otto MJ, Otto MM, Reid C, Sharpe TR, Shum L, Winslow DL, Erickson-Viitanen S (1996) Chem Biol 3:301–314
31. Lu Y, Yang CY, Wang S (2006) J Am Chem Soc 128:11830–11839
32. Davies MN, Toseland CP, Moss DM, Flower DR (2006) BMC Biochem 7:18 doi:10.1186/1471-2091-7-18